

Unveiling atomic-scale features of inherent heterogeneity in metallic glass by molecular dynamics simulations

Y. C. Hu,^{1,2} P. F. Guan,^{3,*} M. Z. Li,⁴ C. T. Liu,² Y. Yang,^{2,†} H. Y. Bai,¹ and W. H. Wang^{1,‡}

¹*Institute of Physics, Chinese Academy of Sciences, Beijing 100190, China*

²*Centre for Advanced Structural Materials, Department of Mechanical and Biomedical Engineering, City University of Hong Kong, Hong Kong, China*

³*Beijing Computational Science Research Center, Beijing 100193, China*

⁴*Department of Physics, Renmin University of China, Beijing 100872, China*

(Received 25 February 2016; revised manuscript received 15 April 2016; published 6 June 2016)

Heterogeneity is commonly believed to be intrinsic to metallic glasses (MGs). Nevertheless, how to distinguish and characterize the heterogeneity at the atomic level is still debated. Based on the extensive molecular dynamics simulations that combine isoconfigurational ensemble and atomic pinning methods, we directly reveal that MG contains flow units and the elastic matrix which can be well distinguished by their distinctive atomic-level responsiveness and mechanical performance. The microscopic features of the flow units, such as the shape, spatial distribution dimensionality, and correlation length, are characterized from atomic position analyses. Furthermore, the correlation between the flow units and the landscape of energy state, free volume, atomic-level stress, and especially the local bond orientational order parameter is discussed.

DOI: [10.1103/PhysRevB.93.214202](https://doi.org/10.1103/PhysRevB.93.214202)

I. INTRODUCTION

Owing to the superior mechanical and physical properties, metallic glasses (MGs) have attracted tremendous attention as promising candidates for structural and functional applications [1–4]. Unfortunately, the unpredicted catastrophic failure stemming from the disordered structure, as the Achilles' heel of MGs, severely restricts their large-scale applications [5–7]. Therefore, the corresponding microstructural origin becomes one of the most important issues in material sciences [5,6,8]. Referring to the deformation mechanism in crystalline solids, establishing a sophisticated structure-property relationship is highly desirable, and a plethora of phenomenological models intending to bridge microstructures and properties have been proposed [9], like free volume [10], shear transformation zones (STZs) [11,12], flow units [13], the geometrically unfavored motifs (GUMs) [4], and the tight-bond cluster model [14]. The common ground of these models is that there are certain local areas behaving differently under external forces compared to their surroundings, which can be termed as “heterogeneity” [15]. Although many experiments and simulations confirmed the inhomogeneous structure of a dynamic nature in MGs recently [16–25], direct revelation of the details of the dynamic heterogeneity is rare and urgent. However, despite early and recent theoretical efforts, it is still difficult to distinguish and characterize the heterogeneity at the atomic level, whether based on static or dynamic properties.

Due to the complicated amorphous state in MGs, the traditional two-order correlation function, i.e. pair correlation function, varies faintly during cooling and loading, which fails in capturing the overall structural amorphousness. Therefore, high-order correlation functions, such as four-point density

correlation function, are necessary and more appropriate to characterize the feature of heterogeneity. However, limited information, especially the local details, can be extracted from synchrotron radiation or neutron scattering experiments, which makes it difficult for us to understand the underlying physics only based on the experimental observations. In this paper, we employed large-scale molecular dynamics (MD) simulations that combine isoconfigurational ensemble and atomic pinning methods to distinguish and characterize the heterogeneity at the atomic level. The microscopic features and behaviors of these well-distinguished regions are revealed and discussed.

II. METHODS

Molecular dynamics simulations are performed using LAMMPS code [26]. The prototypical binary system $\text{Cu}_{50}\text{Zr}_{50}$ was selected for its superior glass-forming ability and simple constituents [27]. A series of simulations based on the $\text{Cu}_{50}\text{Zr}_{50}$ MG constructed by the embedded atom method potential [28], for system sizes of $N = 10\,000$ (S1, $\sim 5.6 \times 5.6 \times 5.6 \text{ nm}^3$) and $N = 1\,600\,000$ (S2, $\sim 131.8 \times 131.8 \times 1.6 \text{ nm}^3$), were performed. To prepare the samples, periodic boundary conditions were applied in three directions. For S1, the sample was first equilibrated at 2000 K for 1 ns. Following this, the sample was quenched to 1 K at a rate of 10^{11} K s^{-1} in the isothermal-isobaric ensemble (NPT) keeping the external pressure at zero. The temperature was controlled by the Nose-Hoover thermostat [29], and the chosen integral time step was 0.002 ps. For the large system S2, in order to avoid potential interface through the strategy of replication, the sample was first equilibrated at 1200 K for 2 ns with the time step of 0.005 ps. The state points below 1200 K were obtained via a stepwise cooling procedure. Each new state point with the interval of 50 K was obtained by quenching simultaneously from the higher temperature. The relaxation time at each temperature

*pguan@csrc.ac.cn

†yonyang@cityu.edu.hk

‡whw@iphy.ac.cn

was 0.5 ns, so the effective cooling rate is 10^{11} K s^{-1} . The ensemble and thermostat of S2 were the same as S1.

In order to directly and effectively distinguish the intrinsic heterogeneities in the MG, we simulated the atomic-level responsiveness and mechanical performance by combining isoconfigurational ensemble and atomic pinning methods [21,30–33]. The static correlation length of the distinguished regions was extracted by the static four-point density correlation function [34,35]. To minimize the temperature-induced thermal fluctuation effect [36,37], the deformation temperature was set at 1 K, at which the temperature-induced thermal fluctuation effect is assumed to be negligible.

III. RESULTS AND DISCUSSION

Figure 1(a) shows the typical shear stress-strain curves of S1 and S2 at 1 K with strain rate of $1.0 \times 10^{-4} \text{ ps}^{-1}$, which is analogous to the previous results [38]. According to the deviation from the linear stress-strain relationship for S2 (also similar for S1), the yield strain is roughly defined as 4%, as shown in Fig. 1(a). In order to unravel the influence of the initial state on the probability of nonaffine atomic motion in the subsequent deformation process, isoconfigurational ensemble introduced by Widmer-Cooper and Harrowell [21] and Widmer-Cooper *et al.* [30] was employed: 100 independent shear deformation simulations were performed, which all started from the same initial configuration but with momenta randomly assigned

from the Maxwell-Boltzmann distribution at the temperature of interest and proceeded until yielding occurred. To quantify the shear deformation at the atomic level, local atomic shear strain $\eta_i^{\text{Mises}}(j)$ of atom i in j th run was calculated, with the reference configuration being the initial undeformed one [39]. Hence, the isoconfigurational ensemble average of the atomic strain for atom i , $\langle \eta_i^{\text{Mises}}(j) \rangle$, can be regarded as the propensity for deformation of particle i in the given initial configuration. This propensity is directly associated with the probability of an atom undergoing a certain nonaffine displacement in a specific configuration. As shown in the contour maps of the same slice (5 \AA , $\sim 2d_{\text{Cu}}$) of S1 for three independent shear runs in Figs. 1(b)–1(d), the mechanical responses are highly heterogeneous under the current circumstance. More importantly, the areas with the large and small nonaffine deformation observed are nearly identical (not absolutely the same) in the visualized snapshots. Similar results were obtained for all 100 runs (see Supplemental Material, Mov. 1, S1, [40]), indicating that we can employ the isoconfigurational ensemble to investigate how these responses under the given loading are determined by the initial configuration. Here, we should emphasize that the nonaffine deformation in the nearly identical regions only occurs in the apparent elastic regime. After yielding, there is a significant variability in the spatial distribution of the nonaffine deformation regions (see Supplemental Material, Mov. 2 for strain 8% and Mov. 3 for strain 12%, S1, [40]). This behavior indicates that the emergence of the nonaffine deformation regions in

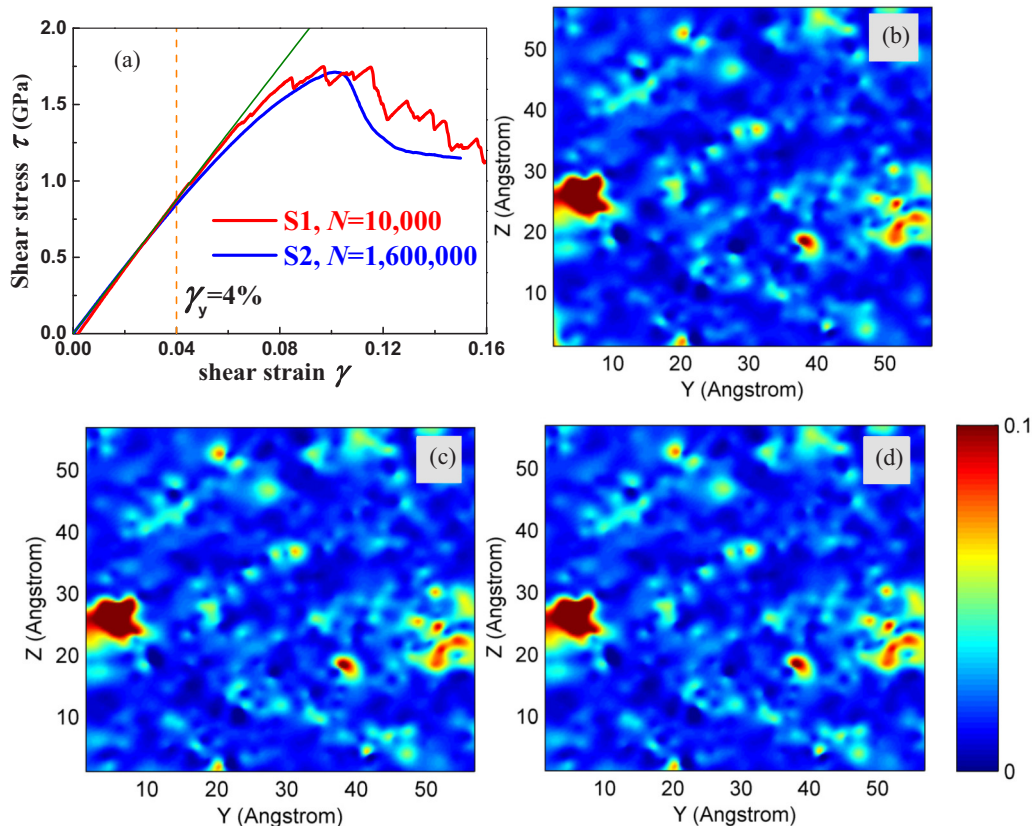


FIG. 1. (a) Shear stress-strain curves of $\text{Cu}_{50}\text{Zr}_{50}$ MG for S1 and S2 at 1 K with strain rate $1.0 \times 10^8 \text{ s}^{-1}$. The yielding strain is about 4%. (b)–(d) Contour maps of the same slice (5 \AA , $\sim 2d_{\text{Cu}}$) from three independent shear runs to the yielding point (4%). The color scale represents the atomic nonaffine displacement revealed by η_i^{Mises} .

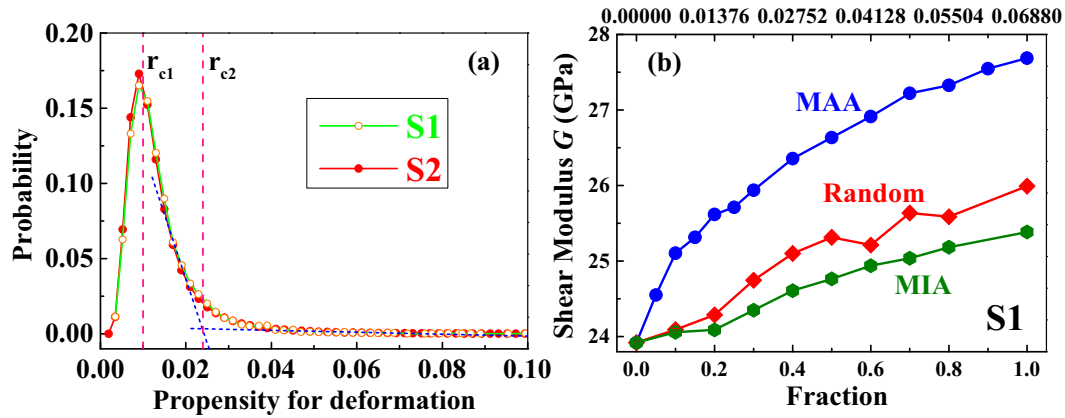


FIG. 2. (a) Probability distributions of propensity for deformation of S1 and S2. (b) Macroscopic shear modulus G of S1 when different numbers of atoms from MAAs, MIAs, or the whole system randomly are pinned. The lower abscissa axis is based on the atom number in MAAs, while the upper one is based on the atom number of the whole system.

the elastic regime is an intrinsic response in MGs. In other words, the inherent heterogeneity can be distinguished by the atomic-level responsiveness under the external stress or strain.

According to the probability distribution of propensity for deformation of S1 and S2 shown in Fig. 2(a), almost no finite-size effect was observed, and thus, we chose two cutoffs, r_{c1} and r_{c2} ($r_{c1} < r_{c2}$), to differentiate soft regions from their elastic surroundings. We define r_{c1} as about the peak value. Obviously, the peak value is smaller than the average value of the system, and it is reasonable to use it for selecting elastic-respond (inactive) atoms. For r_{c2} , we simply define it as the intersection of the tangents of the long tail and the nearly non-Gaussian part [see Fig. 2(a)]. Further explanations on the physical meaning of the cutoff values can be found in the Supplemental Material [40]. The specific values of r_{c1} and r_{c2} are 0.010 and 0.024 for S1 and S2. The cutoffs do not affect our conclusions qualitatively (see Supplemental Material, Figs. S1(c) and S1(d) [40]). Therefore, we propose to define the most active atoms (MAAs, i.e. soft regions) and the most inactive atoms (MIAs, i.e. elastic matrix), respectively, as the atoms that have $\eta_i^{\text{Mises}}(j)$ larger than r_{c2} and smaller than r_{c1} in every independent MD run [41]. Additionally, potential active atoms (PAAs) are also defined as atoms whose local shear strain exceeds r_{c2} at least once during the 100 MD runs. The atom number in the PAA group is larger than that in the MAA group. It means that the atomic-level mechanical responsiveness is still affected by the initial perturbation (the momenta distribution), but the atom number in the MAA group tends to saturate during 100 runs (see Supplemental Material, Fig. S2 [40]). It confirms that the response in the MAA regime is determined by the initial configuration no matter what the perturbation (the momenta distribution) is. As shown in the Supplemental Material, Fig. S3 [40], both the probability distribution of the propensity for deformation and the fraction of MAAs/PAAs/MIAs are insensitive to the applied strain rate. However, the fractions of MAAs and PAAs decrease at lower cooling rates, while MIAs behave in an opposite trend. This indicates that the flow units we defined are determined by the thermal history and are intrinsic to MG (see Supplemental Material, Fig. S4 [40]). In this framework, we also found that there are more Cu than Zr in MAAs and PAAs, while the situation is opposite in MIAs,

indicating that the responsibility of Cu is much stronger than Zr during the mechanical loading in the simulated $\text{Cu}_{50}\text{Zr}_{50}$ MG. Due to the disordered nature of amorphous materials, the local properties vary continuously, and there is no sharp boundary to separate different groups of atoms. What we have done here is to single out three distinct parts, MAAs, PAAs, and MIAs, using a direct method that is impossible in experiments. Here, we should stress that, with the current perturbation-response method, we could directly pick up the atoms which present the highest responsibility to the plastic events during a mechanical deformation and may reveal the possible correlation linking the mechanical behaviors to microstructure in MGs by investigating the features of these atoms.

To understand the roles that MAAs and MIAs played in the deformation of MGs and discover what their microstructural characteristics are [16,18,22], we employed the atomic-pinning method to explore the effects of MAAs and MIAs on the shear modulus G , respectively [16,42]. The process is as follows: to save the computer time, we pinned the same number of atoms from three different groups in S1: MAAs or MIAs or the whole system randomly, and then extracted the macroscopic shear modulus from the shear stress-strain curve. The result is shown in Fig. 2(b), where the atom numbers were normalized by the total atom number in MAAs and the whole system, respectively. Obviously, with increasing number of pinning atoms, the shear moduli are increased by different sensitivities for the three different groups. For MAA pinning, the shear modulus increases rapidly first and then tends to saturate. However, the trends for random pinning and MIA pinning are much weaker, especially for MIA pinning. Since atomic pinning results in pure elastic response of atoms under an external stress, if a MG was homogeneous, the increase in shear moduli should be identical when pinning the same number of atoms wherever they are. Therefore, a significant increase of shear modulus after pinning indicates a softer state or an inelastic response in the initial configuration, such as MAAs. In other words, the relatively small increase caused by the atom pinning in MIAs suggests that these atoms tend to behave in a quasielastic manner without atomic pinning. Hence, the results confirm that MG is inherently heterogeneous and can be distinguished effectively in the MD simulations by

the isoconfigurational ensemble and atomic-pinning methods. The MAA regions which are favorable for plastic events can be defined as flow units, and the MIA region comprises the elastic matrix in MGs [16,22]. However, the thermal histories of MGs could affect the behaviors of heterogeneity and may provide the opportunity to understand the origin of heterogeneity. Since sub- T_g annealing is an effective method for regulating the structure characteristics of MGs by inducing the structural relaxation of the whole system, it becomes more powerful to investigate the evolution of heterogeneity during aging or rejuvenation in MGs by combining it with our methods.

Furthermore, we analyzed the static characteristics of the atoms in the different regions of S2 with an inherent heterogeneity in the MG. The spatial distributions of MAAs, PAAs, and MIAs are shown in Fig. 3. While atoms in the MAA and PAA group form isolated clusters, atoms in the MIA group distribute uniformly in the whole space and form a networklike matrix. From Fig. 3(b), it is amazing that the shape of MAAs is approximately elliptical rather than spherical, and they tend to interconnect in the way resembling “grain boundaries” in crystalline materials. This supports the structural model that MGs can be viewed as disordered solids with flow units (or

liquidlike zones) embedding in the elastic background, without any prehypothetical structural features. For a given network, its dimensionality D_f can be evaluated from $N \sim r^{-D_f}$, where N is the smallest number of boxes with length of r needed to cover the network. Here, D_f of MAAs, PAAs, and MIAs is found to be about 1.34, 1.61, and 2.05 [Fig. 4(a)], respectively, indicating the fractal features of these subregions. Furthermore, it demonstrates that the elastic matrix stacks much more compact in the whole space than the flow units. Within the spirit of four-point density correlation function borrowed from liquid dynamics to extract the static structural length scale [35], we calculated the four-point structure factors $S_{4,M}$ of atoms belonging to a specific group, like MAAs, PAAs, and MIAs

$$S_{4,M}(\mathbf{k}) = \frac{1}{N\rho} \left\langle \sum_{j=1}^{N_M} \sum_{i=1}^{N_M} \exp[-i\mathbf{k} \cdot \mathbf{r}_j(0)] \exp[i\mathbf{k} \cdot \mathbf{r}_i(0)] \right\rangle,$$

where N is total atom number, ρ is the number density, and N_M is the atom number in the considered group. Here, \mathbf{k} and $\mathbf{r}_j(0)$ are the wave vector and position vector of particle j in the initial configuration, respectively. The static correlation

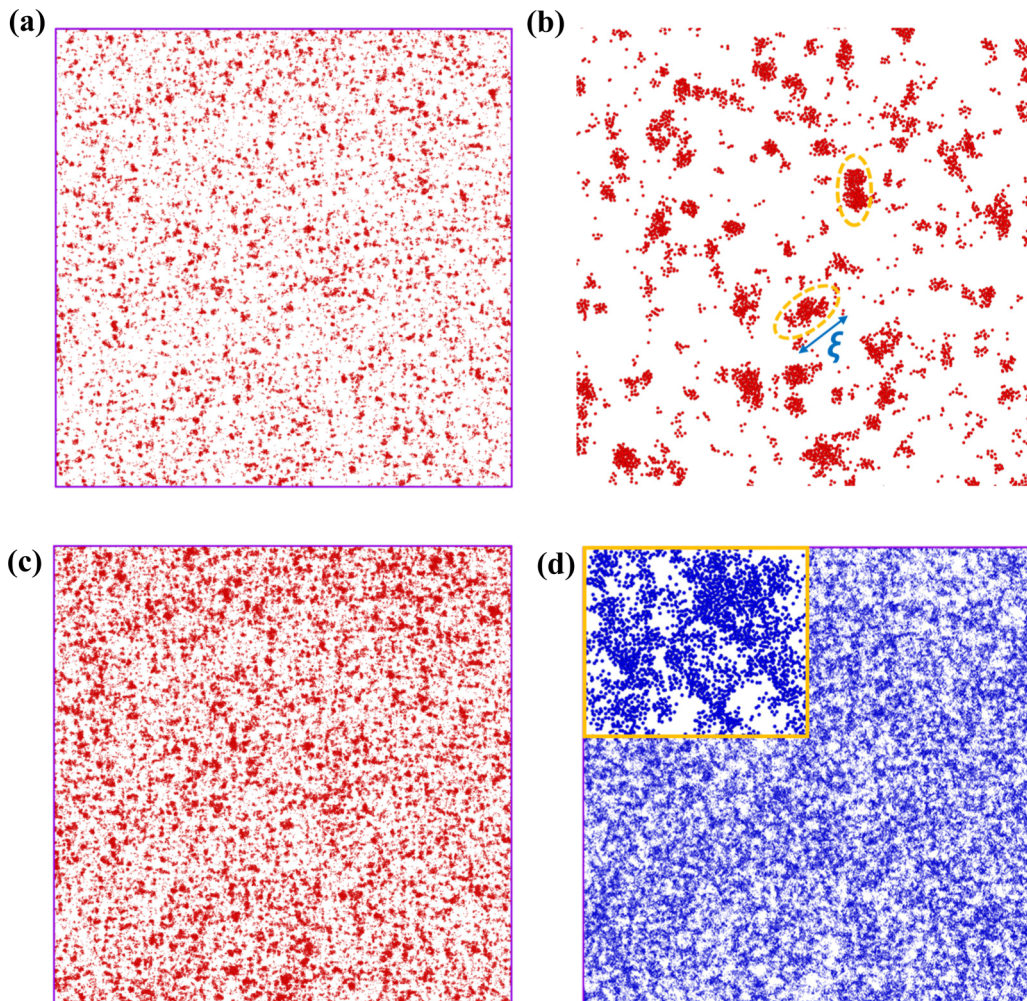


FIG. 3. Snapshots of (a) MAAs, (c) PAAs, and (d) MIAs in the initial configuration of S2. (b) An enlarged region of MAAs that shows flow units are approximately elliptical spatially with a characteristic correlation length ξ . While atoms in MAAs and PAAs form isolated clusters (a)–(c), they are interconnected as shown in the enlarged MIA from the inset of (d). The thickness is ~ 1.6 nm ($\sim 6d_{Cu}$).

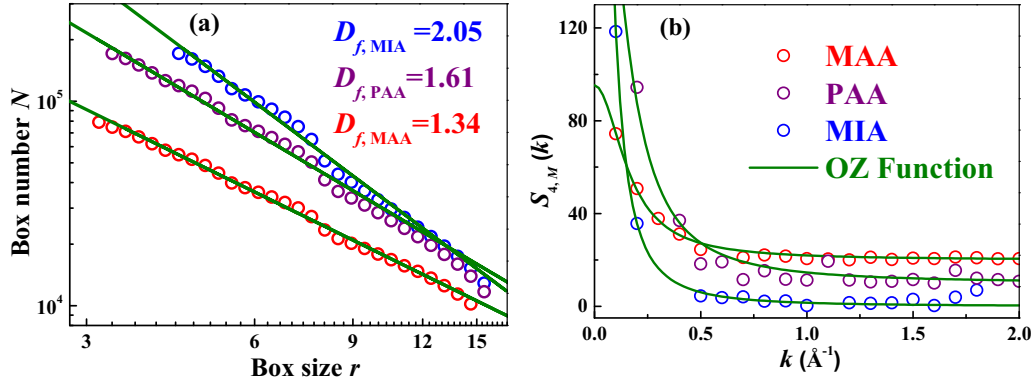


FIG. 4. (a) Fractal dimensionality D_f of MAAs, PAAs, and MIAs computed by the counting box method. The straight lines are power-law fittings: $N \sim r^{-D_f}$. (b) The four-point static structure factors $S_{4,M}$ for MAAs, PAAs, and MIAs. The solid lines are fits to the data with the OZ function to extract static correlation length ξ_M .

length ξ_M is then obtained by fitting the Ornstein-Zernike (OZ) function

$$S_{4,M}(k) = \frac{S_{4,M}(0)}{1 + (k \cdot \xi_M)^2},$$

to the low k values ($k < 2.0 \text{ \AA}^{-1}$) of the structure factor $S_{4,M}(k)$, as shown in Fig. 4(b) [35,43]. Interestingly, the correlation length ξ_M is found to be about 6.1 and 7.0 \AA for MAA and

PAA, respectively, while the value for MIA is much large, $\sim 18.5 \text{ \AA}$. However, this value may correlate to the cutoffs, r_{c1} and r_{c2} , and will be investigated in the future. But, the distinct quantities of ξ_M for the flow units and elastic matrix still support our findings of the inherent heterogeneity in MGs. A rough estimate indicates that the atom number in single flow unit according to ξ_M is around 150, which is close to the estimated STZ volume [44].

In order to characterize the microscopic features of the atoms within different groups and extract the possible correlation linking the mechanical behavior to the initial configuration of MG, we analyzed the free volume (V), potential energy (E), atomic-level stress (S), and bond orientational order (BOO; Q_6) of these atoms in the initial state of S2 [10,45–47]. In particular, the Voronoi volume of each atom was employed to analyze V . We also introduced the deviation from the average to illustrate V and E effectively, according to $\delta_i(A) = A_i^j - \langle A^j \rangle$, where A represents V and E , i denotes the atom index, and j delegates the element type, respectively. Here, $\langle \dots \rangle$ represents an average over the same atom type, i.e. Cu or Zr. The von Mises stress of atom i , $\sigma_{\text{VM}}^i = \sqrt{\frac{1}{2}[(\sigma_{11}^i - \sigma_{22}^i)^2 + (\sigma_{22}^i - \sigma_{33}^i)^2 + (\sigma_{11}^i - \sigma_{33}^i)^2] + 3[(\sigma_{12}^i)^2 + (\sigma_{23}^i)^2 + (\sigma_{13}^i)^2]}$, from the virial stress tensors was extracted to represent S [48]. Voronoi tessellation [47] divides space into a close-packed polyhedral around atoms by constructing bisecting planes along the lines joining the central atom and all its neighbors. In this way, we can obtain the atomic Voronoi volume. Furthermore, to quantitatively describe the bond-orientational symmetry around the center atom, spherical harmonics was employed to calculate the local BOO parameter [46]. The BOO of atom i can be represented by the l -fold symmetry as a $2l + 1$ vector defined as $q_{lm}(i) = \frac{1}{N_i} \sum_1^{N_i} Y_{lm}[\theta(\mathbf{r}_{ij}), \varphi(\mathbf{r}_{ij})]$, where Y_{lm} are the spherical harmonics, N_i is the nearest neighbor number of atom i , and \mathbf{r}_{ij} is the position vector between particle i and j . Then its rotational invariant combination can be extracted according to $Q_l = [\frac{4\pi}{2l+1} \sum_{m=-l}^l |q_{lm}|^2]^{1/2}$. Here, Q_l can be used to define the local BOO parameter and note that $l = 3$ for tetrahedron [49] and $l = 6$ for icosahedron [50].

The probability distributions of these four structural parameters for atoms in MAAs, PAAs, and MIAs are shown in Figs. 5(a)–5(d), respectively. Each distribution of MAAs, PAAs, and MIAs is normalized to its corresponding fraction in the whole sample. The distribution of the atoms in MAAs or PAAs presents obvious trend to the higher potential energy, larger free volume, and bigger atomic-level stress [10,45,51]. It means that the flow units according to our definition were composed of the less stable atoms, which are easy to be activated. More importantly, a larger difference was found in the distribution of Q_6 between the flow units and elastic matrix, which indicates that the BOO parameter is more important or efficient to track the flow units than other geometric/thermodynamic features. Finding an order parameter for amorphous systems is no easy task and extremely vital [52,53],

while Q_6 shown here may be a promising one for MGs, as proposed in the glass transition for other systems, like water and colloids, which deserves further careful research [50]. Furthermore, the different distribution of Q_6 may suggest distinct crystallization behaviors in the MIA and MAA regions. It provides us the opportunity to investigate the behaviors of crystal-glass nanocomposites in the future.

IV. CONCLUSION

In summary, we confirm the inherent heterogeneity in typical $\text{Cu}_{50}\text{Zr}_{50}$ MG by the combining methods of isoconfigurational ensemble and atomic pinning. The flow units and elastic matrix can be differentiated by the atomic-level responsiveness during mechanical loading, which

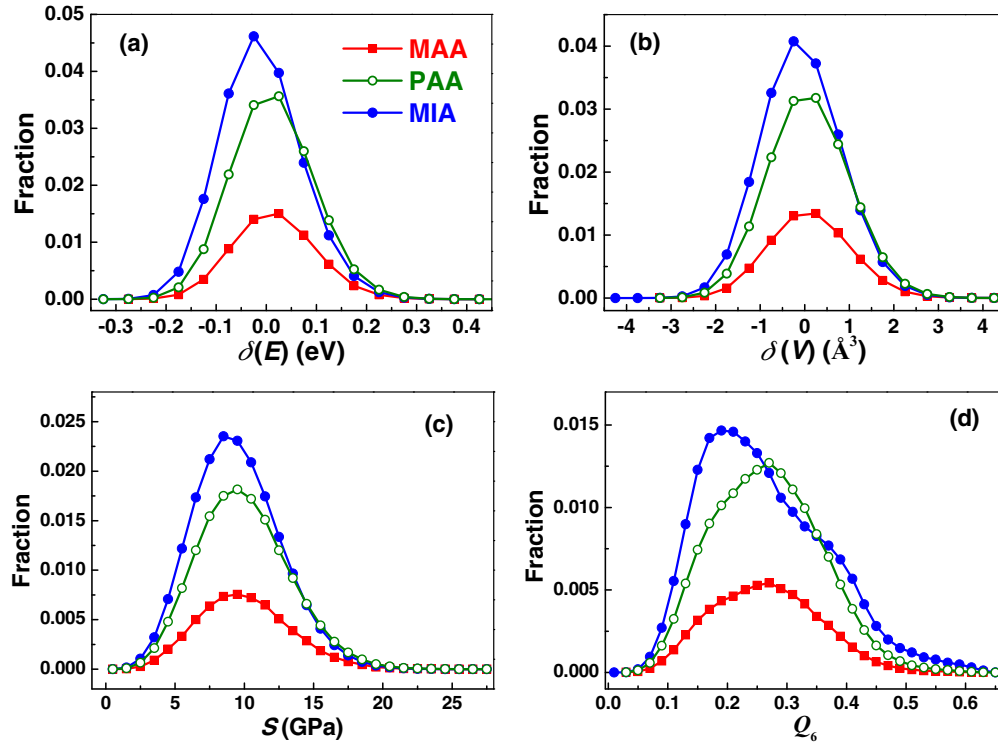


FIG. 5. (a)–(d) Probability distributions of the deviations of potential energy $\delta(E)$, deviations of free volume $\delta(V)$, atomic-level stress S , and local BOO Q_6 for MAAs, PAAs, and MIAs, respectively. Each distribution of MAAs, PAAs, and MIAs is normalized to its corresponding fraction in the whole sample.

contribute differently to the shear modulus of the MG according to our atomic-pinning analyses. In our framework, it was concluded that the flow units are approximately elliptical rather than spherical, and they tend to interconnect in a way resembling “grain boundaries” in crystals. Spatially, their distribution is fractal, with a correlation length of about 7 \AA extracted from the four-point density correlation function. There are also some features from the static structure indicating the higher activity of flow units, such as higher potential energy, free volume, and atomic-level stress. In the past decades, people have tried to find a clear sign for the activation of flow units during mechanical loading just from the static atomic configuration, but it still remains a mystery. Our findings about Q_6 suggest that the potential parameter that could clearly describe the intrinsic heterogeneity in MGs should include the information from bond orientation.

ACKNOWLEDGMENTS

Insightful discussions with H. L. Peng, Q. Wang, H. P. Zhang, L. J. Wang, and B. S. Shang are highly acknowledged. We also thank D. W. Ding, D. Q. Zhao, B. B. Wang, and M. X. Pan for helpful discussions. The financial support of the National Natural Science Foundation of China (Grants No. 51271195, No. 51271197, and No. 5141101072) and the Ministry of Science and Technology of the People’s Republic of China 973 Program (No. 2015CB856800) are appreciated. P.F.G. is also supported by the NSF of China (Grant No. 51571011) and Young “1000-Talents Plan” program of China. Y.Y. is supported by the Hong Kong government through Research Grant Council Grant No. CityU 11214914 and 11207215, and C.T. Liu by RGC Grant No. CityU 102013. We also acknowledge the computational support from the Beijing Computational Science Research Center (CSRC).

- [1] L. Berthier and M. D. Ediger, *Phys. Today* **69**(1), 40 (2016).
- [2] L. Zhong, J. Wang, H. Sheng, Z. Zhang, and S. X. Mao, *Nature* **512**, 177 (2014).
- [3] S. V. Ketov, Y. H. Sun, S. Nachum, Z. Lu, A. Checchi, A. R. Beraldin, H. Y. Bai, W. H. Wang, D. V. Louzguine-Luzgin, M. A. Carpenter, and A. L. Greer, *Nature* **524**, 200 (2015).
- [4] E. Ma, *Nat. Mater.* **14**, 547 (2015).
- [5] C. A. Schuh, T. C. Hufnagel, and U. Ramamurty, *Acta Mater.* **55**, 4067 (2007).
- [6] A. L. Greer, Y. Q. Cheng, and E. Ma, *Mater. Sci. Eng. R: Reports* **74**, 71 (2013).
- [7] W. H. Wang, C. Dong, and C. H. Shek, *Mater. Sci. Eng. R: Reports* **44**, 45 (2004).
- [8] B. A. Sun and W. H. Wang, *Prog. Mater. Sci.* **74**, 211 (2015).
- [9] Y. Q. Cheng and E. Ma, *Prog. Mater. Sci.* **56**, 379 (2011).
- [10] F. Spaepen, *Acta Metall.* **25**, 407 (1977).
- [11] A. Argon, *Acta Metall.* **27**, 47 (1979).
- [12] M. L. Falk and J. S. Langer, *Phys. Rev. E* **57**, 7192 (1998).
- [13] Z. Lu, W. Jiao, W. H. Wang, and H. Y. Bai, *Phys. Rev. Lett.* **113**, 045501 (2014).
- [14] C. Fan, Y. Ren, C. T. Liu, P. K. Liaw, H. G. Yan, and T. Egami, *Phys. Rev. B* **83**, 195207 (2011).

- [15] W. H. Wang, Y. Yang, T. G. Nieh, and C. T. Liu, *Intermetallics* **67**, 81 (2015).
- [16] J. C. Ye, J. Lu, C. T. Liu, Q. Wang, and Y. Yang, *Nat. Mater.* **9**, 619 (2010).
- [17] Y. Yang, J. F. Zeng, J. C. Ye, and J. Lu, *Appl. Phys. Lett.* **97**, 261905 (2010).
- [18] Y. H. Liu, D. Wang, K. Nakajima, W. Zhang, A. Hirata, T. Nishi, A. Inoue, and M. W. Chen, *Phys. Rev. Lett.* **106**, 125504 (2011).
- [19] T. Fujita, Z. Wang, Y. Liu, H. Sheng, W. Wang, and M. Chen, *Acta Mater.* **60**, 3741 (2012).
- [20] Y. Shi and M. L. Falk, *Phys. Rev. Lett.* **95**, 095502 (2005).
- [21] A. Widmer-Cooper and P. Harrowell, *Phys. Rev. Lett.* **96**, 185701 (2006).
- [22] H. Wagner, D. Bedorf, S. Küchemann, M. Schwabe, B. Zhang, W. Arnold, and K. Samwer, *Nat. Mater.* **10**, 439 (2011).
- [23] L. S. Huo, J. F. Zeng, W. H. Wang, C. T. Liu, and Y. Yang, *Acta Mater.* **61**, 4329 (2013).
- [24] M. Li, C. Z. Wang, S. G. Hao, M. J. Kramer, and K. M. Ho, *Phys. Rev. B* **80**, 184201 (2009).
- [25] H. L. Peng, M. Z. Li, B. A. Sun, and W. H. Wang, *J. Appl. Phys.* **112**, 023516 (2012).
- [26] S. Plimpton, *J. Comput. Phys.* **117**, 1 (1995).
- [27] M. B. Tang, D. Q. Zhao, M. X. Pan, and W. H. Wang, *Chin. Phys. Lett.* **21**, 901 (2004).
- [28] Y. Q. Cheng, E. Ma, and H. W. Sheng, *Phys. Rev. Lett.* **102**, 245501 (2009).
- [29] G. J. Martyna, M. L. Klein, and M. Tuckerman, *J. Chem. Phys.* **97**, 2635 (1992).
- [30] A. Widmer-Cooper, P. Harrowell, and H. Fynewever, *Phys. Rev. Lett.* **93**, 135701 (2004).
- [31] C. Cammarota and G. Biroli, *Proc. Natl. Acad. Sci. U.S.A.* **109**, 8850 (2012).
- [32] C. J. Fullerton and R. L. Jack, *Phys. Rev. Lett.* **112**, 255701 (2014).
- [33] S. Karmakar and G. Parisi, *Proc. Natl. Acad. Sci. U.S.A.* **110**, 2752 (2013).
- [34] N. Lačević, F. W. Starr, T. B. Schröder, and S. C. Glotzer, *J. Chem. Phys.* **119**, 7372 (2003).
- [35] C. P. Royall and S. R. Williams, *Phys. Rep.* **560**, 1 (2015).
- [36] P. F. Guan, M. W. Chen, and T. Egami, *Phys. Rev. Lett.* **104**, 205701 (2010).
- [37] W. Liu, H. Ruan, and L. Zhang, *Philos. Mag. Lett.* **93**, 158 (2013).
- [38] Y. Q. Cheng and E. Ma, *Acta Mater.* **59**, 1800 (2011).
- [39] F. Shimizu, S. Ogata, and J. Li, *Mater. Trans.* **48**, 2923 (2006).
- [40] See Supplemental Material at <http://link.aps.org/supplemental/10.1103/PhysRevB.93.214202> for additional information on movies of isoconfigurational ensemble runs, physical meanings of cutoff values, strain rate effects, and cooling rate effects.
- [41] Y. Zhang, C. Z. Wang, F. Zhang, M. I. Mendelev, M. J. Kramer, and K. M. Ho, *Appl. Phys. Lett.* **105**, 151910 (2014).
- [42] W. H. Wang, *Prog. Mater. Sci.* **57**, 487 (2012).
- [43] A. Malins, J. Eggers, C. P. Royall, S. R. Williams, and H. Tanaka, *J. Chem. Phys.* **138**, 12A535 (2013).
- [44] W. L. Johnson, M. D. Demetriou, J. S. Harmon, M. L. Lind, and K. Samwer, *MRS Bull.* **32**, 644 (2007).
- [45] T. Egami, *Prog. Mater. Sci.* **56**, 637 (2011).
- [46] P. J. Steinhardt, D. R. Nelson, and M. Ronchetti, *Phys. Rev. B* **28**, 784 (1983).
- [47] V. A. Borodin, *Philos. Mag. A* **79**, 1887 (1999).
- [48] Y. Fan, T. Iwashita, and T. Egami, *Nat. Commun.* **5**, 5083 (2014).
- [49] Z. Q. Wang and D. Stroud, *J. Chem. Phys.* **94**, 3896 (1991).
- [50] H. Tanaka, *Eur. Phys. J. E* **35**, 113 (2012).
- [51] P. G. Debenedetti and F. H. Stillinger, *Nature* **410**, 259 (2001).
- [52] W. Xu, M. T. Sandor, Y. Yu, H. B. Ke, H. P. Zhang, M. Z. Li, W. H. Wang, L. Liu, and Y. Wu, *Nat. Commun.* **6**, 7696 (2015).
- [53] Y. C. Hu, F. X. Li, M. Z. Li, H. Y. Bai, and W. H. Wang, *Nat. Commun.* **6**, 8310 (2015).